RESEARCH ARTICLE

Check for updates

Bioassay-guided isolation of hepatoprotective lignans from *Vernonia cinerea*: DeepSAT-driven structural elucidation and predictive mechanistic insights against drug-induced liver injury†

Mu Li,‡[abc] Meng-Ke Zhang,‡[bc] Xin Song,[d] Yu-Ting Zhong,[c] Ming-An Gui,[a] Jie Ping,*[d] You-Sheng Cai [ID] *[ac] and Rui-Ying Yuan*[a]

Three new dibenzylbutane lignans, vernolignans A–C (**1**–**3**), along with three known compounds (**4**–**6**), were isolated from *Vernonia cinerea* through a bioactivity-guided isolation process. The planar structures of the new compounds (**1**–**3**) were elucidated through comprehensive analysis of HR-ESI-MS and 1D/2D NMR data, with the assistance of AI-based structure annotation tool DeepSAT. The absolute configurations of **1**–**3** were determined by comparing the experimental and calculated ECD spectra. Compounds **2** and **3** exhibited significant improvements in cell viability and attenuated acetaminophen-induced alanine aminotransferase levels in murine hepatocytes at 20 μM. Bioinformatics analysis and molecular docking suggested that BRAF might be a potential target for these lignans.

1. Introduction

Drug-induced liver injury (DILI) is a major cause of liver dysfunction and remains a critical challenge in clinical medicine.[1] DILI can result from the direct hepatotoxicity of drugs or an idiosyncratic immune response, often leading to acute liver failure if not properly managed.[2] Acetaminophen (APAP) hepatotoxicity, a prototypical example of DILI, accounts for nearly 50% of acute liver failure (ALF) cases in the United States and Europe,[3,4] underscoring its significant impact on public health. Due to the complex pathogenesis and limited effective treatments, there is a growing interest in identifying hepatoprotective agents from natural sources. Natural products have been extensively explored for their therapeutic potential, and numerous bioactive compounds have been discovered with protective effects against liver injury.[5] For instance, silymarin, a flavonolignan complex from *Silybum marianum*, has been widely used as a hepatoprotective agent, demonstrating efficacy in mitigating anti-tuberculosis drug-induced liver injury.[6,7]

Vernonia cinerea (L.), commonly known as little ironweed, is a medicinal plant traditionally used across Asia for treating various diseases, including malaria, infertility, skin infections, and liver disorders.[8–10] Recent pharmacological studies have revealed its diverse bioactivities, including antioxidant, anti-inflammatory, anti-tumor, anti-bacteria, and hepatoprotective effects.[11–14] Clinical studies in Thailand have demonstrated its efficacy in smoking cessation.[15–17] In chronic nicotine-treated rats, *V. cinerea* has also shown hepatoprotective effects against nicotine-induced liver damage.[18]

In our previous investigations on the chemical constituents of *V. cinerea*, a series of novel sesquiterpene lactones with unique skeletons were isolated, some of which exhibited significant anti-inflammatory activities.[19,20] Building on the anti-inflammatory and hepatoprotective properties of *V. cinerea*, and as part of our ongoing search for natural compounds with hepatoprotective activity,[21] a bioactivity-guided fractionation was conducted. This approach led to the identification of several fractions with significant hepatoprotective effects. Further chemical investigation of these fractions, aided by the DeepSAT platform (**https://deepsat.ucsd.edu**),[22] resulted in the discovery of three new dibenzylbutane lignans, vernolignans A–C (**1**–**3**), along with three known compounds (**4**–**6**) (Fig. 1). Bioassay results demonstrated that compounds **2** and **3** significantly improved cell viability and attenuated acetaminophen-induced alanine aminotransferase levels in murine hepatocytes. Further bioinformatics analysis and

[a] *Department of Medicament, College of Medicine, Tibet University, Lhasa 850000, China. E-mail: 2627478@qq.com*
[b] *Department of Pharmacy, Renmin Hospital of Wuhan University, Wuhan 430060, China. E-mail: mengke@whu.edu.cn*
[c] *Key Laboratory of Combinatorial Biosynthesis and Drug Discovery, Ministry of Education and School of Pharmaceutical Sciences, Wuhan University, Wuhan, 430071, China. E-mail: cysh2002@whu.edu.cn*
[d] *Department of Pharmacology, School of Basic Medical Sciences, Wuhan University, Wuhan 430071, China. E-mail: pingjie@whu.edu.cn*
† Electronic supplementary information (ESI) available. See DOI: **https://doi.org/10.1039/d5md00331h**
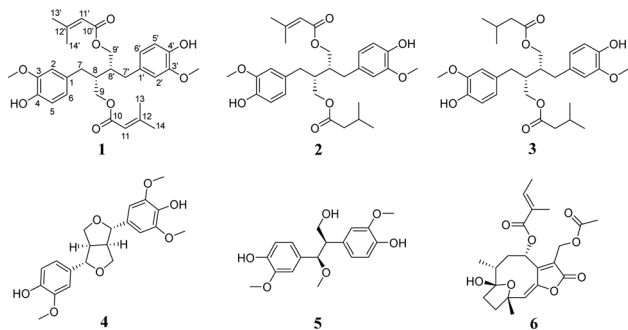‡ These authors contributed equally.

Fig. 1 The structures of compounds **1**–**6**.

molecular docking suggested that BRAF could be a potential target for the active lignans.

2. Materials and methods

2.1 General experimental procedures

Optical rotations were measured on a PerkinElmer Model 341 polarimeter. ECD spectra were acquired on a Chirascan V100 spectropolarimeter. NMR data were recorded with Bruker AVANCE NMR spectrometers at 400 or 600 MHz. HR-ESI-MS spectra were obtained on a ThermoFisher mass spectrometer (LTQ Orbitrap XL). Preparative high-performance liquid chromatography (HPLC) separations were performed on a Hanbang NP7000 series HPLC with UV detector and a semipreparative RP C_{18} column (5 μm, 10 × 250 mm, Sepax GP-C-18, America) at a flow rate of 3 mL min^{-1}. Size-exclusion chromatography was conducted with Sephadex LH-20 (Pharmacia, Sweden). Column chromatography was performed with silica gel (200–300 mesh, Anhui Liangchen Guiyuan Material Ltd., P. R. China).

2.2 Plant material

The fresh whole plants of *V. cinerea* were collected from Meilin town, Puning, Guangdong province, China, in September 2022. The plant was authenticated by Dr. Mengke Zhang, Renmin Hospital of Wuhan University. A voucher specimen (no. VC 202209) was deposited at the Natural Product Chemistry Laboratory, Renmin Hospital of Wuhan University.

2.3 Extraction, isolation and purification

The dried whole plants of *V. cinerea* (25 kg) were powdered and extract with 85% ethanol under reflux three times, each for 3 h. The filtrate was concentrated under reduced pressure to afford a crude extract (1.2 kg). The extract was suspended in water and partitioned with petroleum ether, dichloromethane, and ethyl acetate, successively. The dichloromethane-soluble fraction (422 g) was subjected to a silica gel chromatography column, eluted with a gradient of petroleum ether–ethyl acetate (from 10 : 1 to 0 : 1), yielding 24 fractions (A–X).

Fraction F (2.2 g) was separated by Sephadex LH-20 column chromatography (CH_2Cl_2/MeOH, 1 : 1, v/v) to yield seven parts (F1–F7). Subfraction F4 (190 mg) was purified by semi-preparative HPLC (65% MeCN, 3.0 mL min^{-1}) to afford **1** (13 mg, t_R = 20.0 min), **2** (4 mg, t_R = 22.2 min), **3** (1 mg, t_R = 24.3 min) and **6** (26 mg, t_R = 11.4 min). Fraction G (3 g) was separated by Sephadex LH-20 column chromatography (CH_2Cl_2/MeOH, 1 : 1, v/v) to yield ten parts (G1–G10). Subfraction G3 (600 mg) was subjected to a silica gel column (PE/EA, 3 : 1–1 : 2, v/v) to yield seven parts (G3a–G3g). Subfraction G3f (60 mg) was separated by semipreparative HPLC (60% MeOH, 3.0 mL min^{-1}) to afford **4** (3 mg, t_R = 22.1 min) and **5** (0.5 mg, t_R = 12.1 min).

2.4 Extraction, isolation and purification

Vernolignan A (1). Colorless oil; $[\alpha]_D^{20}$ −54.7 (*c* 0.1, MeOH); ECD {MeOH, *c* = 1.89 × 10^{-3} M}, λ_{max} (Δε): 227 (−2.11), 210 (+2.84), 193 (−3.88) nm; ^{1}H (400 MHz, CD$_3$OD) and ^{13}C NMR data (150 MHz, CD$_3$OD), see Table 1; HR-ESI-MS *m/z* 525.2467 [M–H]$^-$ (calcd for $C_{30}H_{37}O_8^-$ 525.2493).

Vernolignan B (2). Colorless oil; $[\alpha]_D^{20}$ −48.0 (*c* 0.1, MeOH); ECD {MeOH, *c* = 1.89 × 10^{-3} M}, λ_{max} (Δε): 228 (−3.93), 208 (+7.96), 196 (−17.50) nm; ^{1}H (600 MHz, CD$_3$OD) and ^{13}C (150 MHz, CD$_3$OD) data see Table 1; HR-ESI-MS *m/z* 527.2613 [M–H]$^-$ (calcd for $C_{30}H_{39}O_8^-$ 527.2650).

Vernolignan C (3). Colorless oil; $[\alpha]_D^{20}$ −96.7 (*c* 0.1, MeOH); ECD {MeOH, *c* = 1.89 × 10^{-3} M}, λ_{max} (Δε): 226 (−2.30), 208 (+4.97), 195 (−13.47) nm; ^{1}H (600 MHz, CD$_3$OD) and ^{13}C (150 MHz, CD$_3$OD) data see Table 1; HR-ESI-MS *m/z* 529.2764 [M–H]$^-$ (calcd for $C_{30}H_{41}O_8^-$ 529.2807).

2.5 ECD calculation

For the ECD spectral calculations of compound **1**, the sets of stable conformers obtained by the chemical shift calculations using Spartan′20 were further optimized with the Gaussian 09 software package at the B3LYP/6-31G (d,p) level under vacuum conditions. The low energy conformations were further optimized with B3LYP/6-311G (2d,p) level under vacuum conditions. The obtained stable conformers were subjected to UV/ECD calculations with time-dependent density functional theory (TD-DFT) methods at the B3LYP/6-311G (2d,p) level. The calculated spectra were combined by considering the Boltzmann distribution. The wavelengths of the calculated UV spectrum were corrected based on the experimental UV spectrum, and the same correction was applied to the ECD wavelengths.

2.6 Cell culture and treatment

Murine hepatocytes AML-12 were cultured in DMEM/F12 (Servicebio, Wuhan, China) supplemented with 10% FBS, ITS (5 mg mL^{-1} insulin, 5 mg mL^{-1} transferrin, and 5 ng mL^{-1} selenium), 1% penicillin–streptomycin solution and 40 ng mL^{-1} dexamethasone at 37 °C with 5% CO$_2$. The AML-12 cells were plated into 96-well plates for 12 h and then incubated with different concentrations of drugs in the presence of 10

Table 1 ^{1}H and ^{13}C NMR data of compounds **1–3** (CD$_3$OD, δ in ppm, J in Hz)

No	**1**[a] δ_H	δ_C	**2**[b] δ_H	δ_C	**3**[b] δ_H	δ_C
1		132.9		132.8		132.7
2	6.56 d (2.0)	113.3	6.54 d (1.9)	113.2	6.54 d (2.0)	113.7
3		148.9		148.9		148.9
4		145.7		145.8		145.8
5	6.67 d (8.0)	115.9	6.66 dd (7.9, 1.2)	115.9	6.66 d (8.0)	115.9
6	6.51 dd (8.0, 2.0)	122.6	6.50 m	122.6	6.51 dd (8.0, 2.0)	122.6
7	2.60 dd (13.9, 7.2)	36.0	2.60 m	35.9	2.61 dd (13.8, 7.0)	35.9
	2.66 dd (13.9, 7.6)		2.65 m		2.65 dd (13.8, 7.7)	
8	2.12 m	41.3	2.08 m	41.2	2.08 m	41.3
9	4.05 dd (11.3, 5.5)	64.7	3.99 m	65.5	3.99 dd (11.2, 5.9)	65.4
	4.21 dd (11.3, 6.0)		4.27 dd (11.2, 5.7)		4.27 dd (11.2, 5.7)	
10		168.2		174.8		174.8
11	5.72 m	116.7	2.20 d (7.5)	44.4	2.21 d (7.1)	44.4
12		158.8	2.06 m	27.0	2.08 m	27.0
13	1.93 s	27.4	0.97 d (0.9)	22.8	0.97 d (6.6)	22.8
14	2.18 s	20.4	0.96 d (0.9)	22.8	0.97 d (6.6)	22.8
3-OCH$_3$	3.74 s	56.1	3.73 s	56.2	3.74 s	56.2
1′		132.9		132.8		132.7
2′	6.56 d (2.0)	113.3	6.55 d (1.9);	113.3	6.54 d (2.0)	113.7
3′		148.9		148.9		148.9
4′		145.7		145.8		145.8
5′	6.67 d (8.0)	115.9	6.66 dd (7.9, 1.2)	115.9	6.66 d (8.0)	115.9
6′	6.51 dd (8.0, 2.0)	122.6	6.50 m	122.6	6.51 dd (8.0, 2.0)	122.6
7′	2.60 dd (13.9, 7.2)	36.0	2.60 m	36.0	2.61 dd (13.8, 7.0)	35.9
	2.66 dd (13.9, 7.6)		2.65 m		2.65 dd (13.8, 7.7)	
8′	2.12 m	41.3	2.08 m	41.4	2.08 m	41.3
9′	4.05 dd (11.3, 5.5)	64.7	4.04 m	64.7	3.99 dd (11.2, 5.9)	65.4
	4.21 dd (11.3, 6.0)		4.21 dd (11.3, 6.1)		4.27 dd (11.2, 5.7)	
10′		168.2		168.1		174.8
11′	5.72 m	116.7	5.72 s	116.7	2.21 d (7.1)	44.4
12′		158.8		158.9	2.08 m	27.0
13′	1.93 s	27.4	1.93 s	27.4	0.97 d (6.6)	22.8
14′	2.18 s	20.4	2.18 s	20.4	0.97 d (6.6)	22.8
3′-OCH$_3$	3.74 s	56.1	3.74 s	56.2	3.74 s	56.2

[a] Spectra were recorded at 400 MHz for ^{1}H NMR and 150 MHz for ^{13}C NMR. [b] Spectra were recorded at 600 MHz for ^{1}H NMR and 150 MHz for ^{13}C NMR.

mM acetaminophen for 12 h *in vitro*. Drugs was dissolved in the culture medium containing 0.5% DMSO. After treatment, the cells were incubated with 3-(4,5-dimethyl-2-thiazolyl)-2,5-diphenyl-2H-tetrazolium bromide (MTT 5 mg mL^{-1}) for 4 h. Finally, the absorbance was detected at 490 nm using a microplate reader. Cellular supernatant was collected 12 h after acetaminophen treatment. Cellular supernatant alanine aminotransferase (ALT) activities were measured using reagent kits from Nanjing Jiangcheng (Nanjing, China).

2.7 Bioinformatics analysis

The pathways and biological processes were enriched by KEGG and GO with clusterProfiler package in R (v.4.3.2). In addition, the network was constructed using Cytoscape (v.3.9.0) and STRING database.

2.8 Molecular docking study

The crystal structures of BRAF (8QQG), PTPN11 (7JVM), JAK2 (5WIJ), NFE2L2 (2DYH), MAP2K1 (4AE2), PIK3CG (2A5U), MAPK14 (5ETI), RAF (3OMV), and RPS6KB1 (4LSJ) were obtained from the RCSB Protein Data Bank and prepared using

the Protein Preparation Wizard in Schrödinger (Schrödinger LLC, New York, NY, 2021). After removing all crystal water molecules, the structures were minimized using the OPLS_2005 force field, with all other parameters set to the default values. Meanwhile, the 3D configurations of the compounds were crafted using Chem3D Ultra 12.0 software (conforming to the Chemical Structure Drawing Standard, CambridgeSoft 14.0). These structures were then subjected to energetic minimization through the MMFF94 force field, with 5000 iterations and a minimal root-mean-squared gradient of 0.10.

2.9 Statistical analysis

All data were analyzed using IBM SPSS Statistics 25 software (IBM Corp., USA). One-way analysis of variance (ANOVA) was performed, followed by homogeneity of variance testing and *post hoc* comparisons. A *p*-value of less than 0.05 was considered statistically significant.

3. Results and discussion

Bioactivity-guided fractionation: Fractions A–J were evaluated for their hepatoprotective activities. Compared to the APAP

group, all fractions were able to ameliorate APAP-induced apoptosis and significantly improve the survival rate of AML-12 cells. Notably, fractions E, F, and G demonstrated the most pronounced effects. The survival rates of AML-12 cells treated with fractions E, F, and G were significantly higher than those in both the APAP and control groups (Fig. S1†). These results suggested that fractions E, F, and G might contain active ingredients that promote hepatocyte proliferation. Guided by these preliminary results, fractions F and G were further isolated. Fraction F was separated into 7 subfractions (F1–F7) by Sephadex LH-20 column chromatography. Then, the hepatoprotective activities of subfractions F2–F7 were evaluated. Subfractions F2, F3, F4, and F7 significantly improved the survival rate of AML-12 cells under APAP-induced toxicity (Fig. S2†). Subsequently, subfractions F4 and G3 were further isolated, from which compounds **1**–**6** were obtained.

Preliminary DeepSAT analysis: DeepSAT is a neural network-based tool designed to accelerate the identification of molecular structures using NMR spectra.[22] By analyzing ^{1}H–^{13}C HSQC spectra, DeepSAT predicts chemical fingerprints, molecular weights, and structure classes, enabling efficient searches for similar molecules in chemical databases.[23,24] It can significantly accelerate the process of structure elucidation, making it a valuable tool for drug discovery and natural product research.[25] The subfraction F4 was dissolved in methanol-d_4, and its HSQC spectrum was acquired and analyzed using DeepSAT. The DeepSAT result predicted that the probability of the sample being sesquiterpenoid was 68.94% (Fig. 2). Subsequent separation results confirmed this prediction, as the main constituent of subfraction F4, compound **6**, was indeed identified as a sesquiterpenoid.

Previous studies have primarily utilized DeepSAT to analyze HSQC spectra of pure compounds for assisting in structural elucidation.[26,27] In this study, we attempted to apply DeepSAT to analyze the HSQC spectrum of a mixture. The predicted result was completely consistent with the structural type of the major component ultimately isolated. This positive outcome suggests that, in addition to assisting in the interpretation of NMR spectra, DeepSAT holds potential for predicting the chemical type of major components in mixtures. However, the accuracy of its
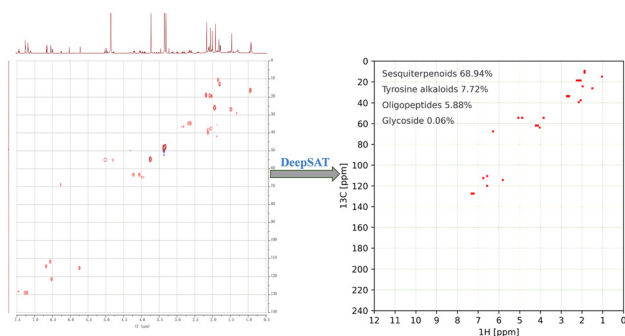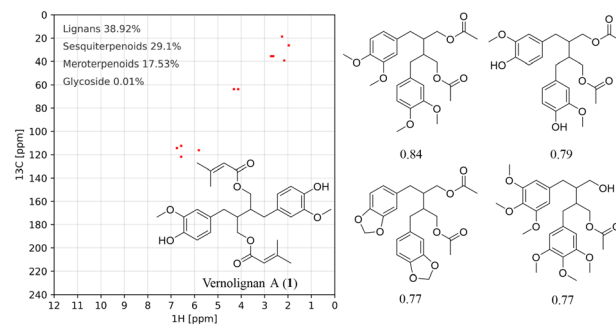

Fig. 3 DeepSAT results of vernolignan A (**1**).

predictions may deeply rely on the percentage of the major component in the mixture. When the proportion of the major component in the mixture is not sufficiently high, the interference signals in the HSQC spectrum will become pronounced, which will lead to a significant reduction in the reliability of the prediction results.

Structure identification: DeepSAT was used to predict the structure of compound **1**. The list of correlation peaks obtained from the multiplicity edited HSQC spectrum of **1** was utilized in DeepSAT to provide the similar compounds along with their cosine score. DeepSAT results (Fig. 3) indicated that compound **1** has a 38.92% probability of belonging to the lignan class and a 46.64% probability of belonging to the terpenoid class. This prediction suggested that the structure of compound **1** may possess fragments of both lignans and terpenoids. Detailed analysis of the NMR spectra of **1** further confirmed this deduction.

Vernolignan A (**1**) was obtained as a colorless oil. Its molecular formula was determined as $C_{30}H_{38}O_8$ based on the ion peak at m/z [M–H]$^-$ 525.2467 (calcd for $C_{30}H_{37}O_8^-$ 525.2493), indicating 12 degrees of unsaturation. In contrast to the HR-ESI-MS result, the ^{13}C NMR spectrum of **1** only displayed 15 carbon resonances, suggesting compound **1** possess a symmetrical structure. The ^{1}H and ^{13}C NMR spectra of **1** (Table 1) demonstrated the typical resonances of 1,3,4-trisubstituted phenyl ring at δ_H 6.67 (1H, d, J = 8.0 Hz, H-5), 6.56 (1H, d, J = 2.0 Hz, H-2), and 6.51 (1H, dd, J = 8.0, 2.0 Hz, H-6); δ_C 148.9 (C-3), 145.7 (C-4), 132.9 (C-1), 122.6 (C-6), 115.9 (C-5), and 113.3 (C-2).

The HMBC correlations (Fig. 4) from H-2 to C-4/C-6, from H-5 to C-1/C-3, and from H-6 to C-2/C-5 further confirmed this deduction, and the correlations from 3-OCH$_3$ to C-3 indicated that the methoxy group to be attached to C-3. Detailed analysis of the ^{1}H and ^{13}C NMR resonances at δ_H
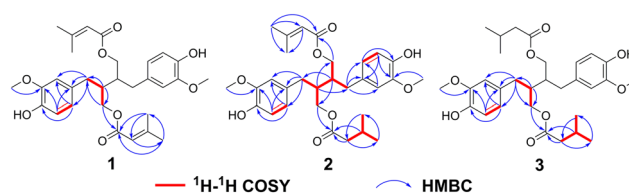

Fig. 2 DeepSAT results of subfraction F4.

Fig. 4 Key ^{1}H–^{1}H COSY and HMBC correlations of compounds **1**–**3**.

5.72 (1H, s, H-11), 2.18 (3H, d, J = 1.4 Hz, H$_3$–14), and 1.93 (3H, d, J = 1.4 Hz, H$_3$–13); δ_C 168.2 (C-10), 158.8 (C-12), 116.7 (C-11), 27.4 (C-13), and 20.4 (C-14) revealed the presence of a senecioyl moiety, which was confirmed by the HMBC correlations from H-11 to C-13/C-14, H$_3$-13 to C-10/C-11/C-14, and H$_3$-14 to C-10/C-11/C-13. The spin system of C-7/C-8/C-9 were recognized by the ^{1}H–^{1}H COSY correlations between δ_H 2.66 (1H, dd, J = 13.9, 7.6 Hz, H-7), 2.60 (1H, dd, J = 13.9, 7.2 Hz, H-7), 2.12 (1H, m, H-8), 4.21 (1H, dd, J = 11.3, 6.0 Hz, H-9) and 4.05 (1H, dd, J = 11.3, 5.5 Hz, H-9). The connection between C-1 and C-7 was supported by the HMBC correlations from H$_2$-7 to C-2/C-6. The location of the senecioyl moiety was determined based on the HMBC correlations observed between H$_2$-9 and C-10. Subsequently, the two symmetrical parts of the molecule were connected through the two non-bonded methine carbons, C-8 and C-8′. Then, the planar structure of **1** was established.

There are two chiral centers in the structure of **1**, theoretically affording four possible absolute configurations. However, the 8S,8′R and 8R,8′S configurations exhibit no chirality due to intramolecular symmetry. Considering the optical activity of compound **1**, electronic circular dichroism (ECD) calculations were performed specifically for the 8S,8′S and 8R,8′R configurations. The experimental data of **1** displayed positive Cotton effect at 210 ($\Delta\varepsilon$ +2.84) nm and negative Cotton effects at 227 ($\Delta\varepsilon$ −2.11) and 193 ($\Delta\varepsilon$ −3.88) nm, which showed excellent agreement with the calculated ECD spectrum for the 8R,8′R configuration (Fig. 5). Thus, the absolute configuration of compound **1** was assigned as 8R,8′R.

Vernolignan B (**2**) was isolated as a colorless oil. Its molecular formula was determined as C$_{30}$H$_{40}$O$_8$ based on a protonated molecule peak at m/z 527.2613 [M−H]$^-$ (calcd for C$_{30}$H$_{39}$O$_8^-$ 527.2650). Analysis of the ^{1}H and ^{13}C NMR spectra of **2** revealed similarities to those of **1**. In addition to the resonances displayed in the spectra of **1**, the NMR spectra of **2** displayed resonances consistent with a isovaleryl moiety at δ_H 2.20 (2H, d, J = 7.5 Hz, H$_2$-11), 2.06 (1H, m, H-12), 0.97

(3H, d, J = 0.9 Hz, H$_3$-13) and 0.96 (3H, d, J = 0.9 Hz, H$_3$-14); δ_C 174.8 (C-10), 44.4 (C-11), 27.0 (C-12), and 22.8 (C-13, C-14), indicating that one of the senecioyl moieties in **1** was replaced by a isovaleryl moiety in **2**. This speculation was confirmed by the ^{1}H–^{1}H COSY correlations between H$_2$-11, H-12, and H$_3$-13, and by the HMBC correlations from H$_2$-11 to C-13/C-14, from H-12 to C-10, from H$_3$-13/H$_3$-14 to C-11/C-14. The HMBC correlations from H$_2$-9 to C-10 proved the isovaleryl moiety attached to C-9.

The experimental ECD spectrum of **2** displayed positive Cotton effect at 208 ($\Delta\varepsilon$ +7.96) nm and negative Cotton effects at 228 ($\Delta\varepsilon$ −3.93) and 196 ($\Delta\varepsilon$ −17.50) nm, which closely resemble those of **1** (Fig. 5). Therefore, the absolute configuration of **2** was determined as 8R,8′R by considering the biogenic synthesis pathway and similar Cotton effects.

Vernolignan C (**3**) was obtained as a colorless oil and gave a molecular ion at m/z 529.2764 [M−H]$^-$ (calcd for C$_{30}$H$_{41}$O$_8^-$ 529.2807). The ^{1}H and ^{13}C NMR spectra of **3** are closely resembled those of **1**. The major differences were that the NMR spectra of **3** demonstrated resonances attribute to an isovaleryl moiety, instead of the senecioyl moiety in **1**. Detailed analysis of the 2D NMR spectra of **3** further verified this inference. Comparative assessment established that the planar structure of **3** aligns with 8,8-bis-dihydroconifery-lalkohol-diisovalerat.[28] The absolute configuration of **3** was determined as 8R,8′R by comparing the ECD spectrum with those of **1**.

The known compounds **4**–**6** (Fig. 1) were identified as (+)-medioresinol (**4**),[29] 4,4′-((1R,2R)-3-hydroxy-1-methoxypro-pane-1,2-diyl)bis(2-methoxyphenol) (**5**),[30,31] and 8α-tigloyloxyhirsutin-13-O-acetate (**6**)[32] by comparing their physical and spectroscopic data with those reported in the literature.

The hepatoprotective activities of compounds **1**–**4** were assessed *in vitro* (Fig. 6A). In this assay, all four compounds (**1**–**4**) effectively mitigated APAP-induced cytotoxicity in AML-12 murine hepatocytes, resulting in a significant increase in cell viability. Compounds **1**, **3**, and **4** exhibited a concentration-dependent protective effect, whereas compound **2** demonstrated maximal activity at 5 μM, with a slight decline in AML-12 cell viability at higher concentrations. This decline may be attributed to the peak hepatoprotective efficacy of compound **2** at 5 μM, beyond which potential mild cytotoxic effects may have emerged, leading to reduced cell viability. Furthermore, compounds **1**, **2**, and **3** significantly decreased ALT level, with compounds **2** and **3** displaying superior efficacy compared to the positive control, N-acetylcysteine (NAC) (Fig. 6B). These results suggested that lignans isolated from *V. cinerea* may have protective effects in DILI.

Considering compounds **1**–**3** shared the same structural framework, compound **1** was selected for target prediction, identifying 180 potential targets using the Swiss target prediction and SuperPred databases. To further explore its relevance to DILI, a total of 8547 DILI-associated targets were retrieved from the OMIM and GeneCards databases. By intersecting these datasets, 164 genes were identified for pathway analysis. Gene ontology (GO) enrichment analysis
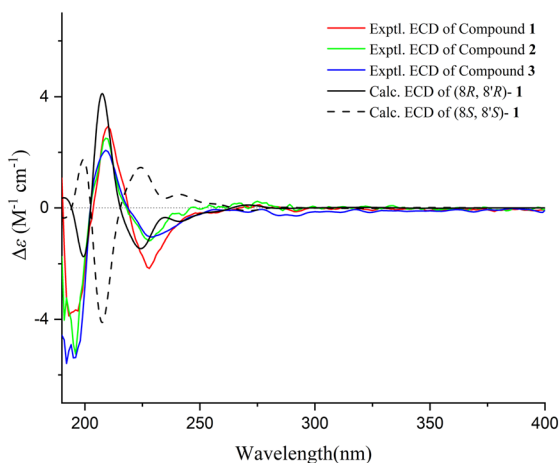

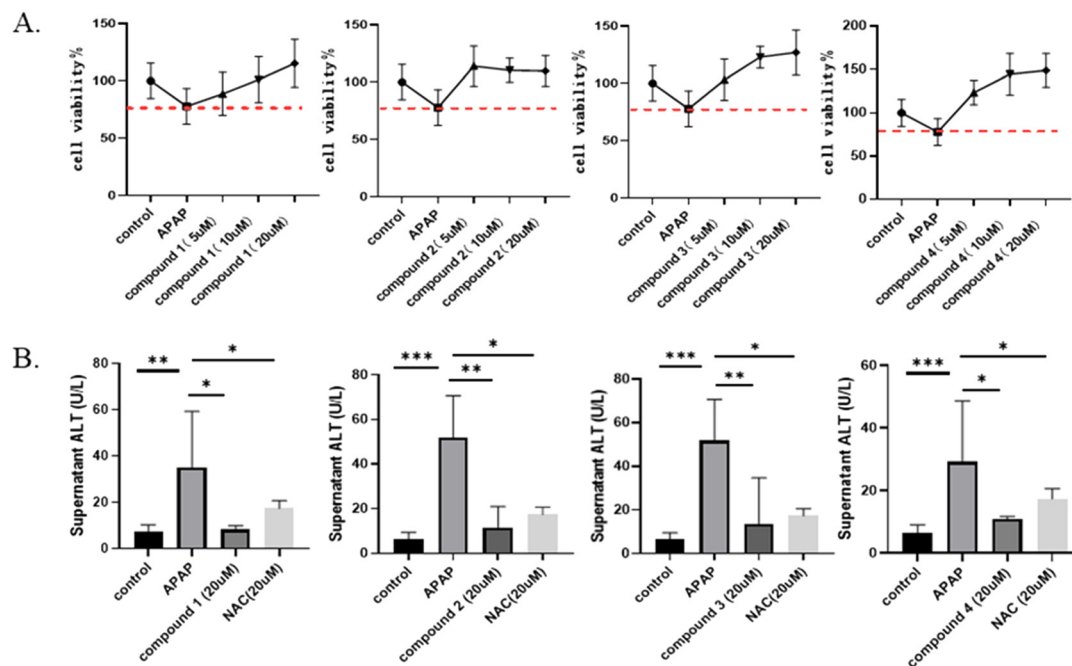**Fig. 5** Experimental and calculated ECD spectra of compound **1**–**3**.

Fig. 6 Protective effects of compounds **1**–**4** on DILI. (A) Effects of compounds **1**–**4** on the survival rate of AML-12 cells in APAP-induced cytotoxicity. (B) Effects of compounds **1**–**4** on ALT levels in DILI. Data were presented as mean ± SD. *$P < 0.05$, **$P < 0.01$, ***$P < 0.001$.

(Fig. S31†) highlighted biological processes such as the positive regulation of the MAPK cascade, ERK1 and ERK2 signaling pathways, and protein kinase activity, which are implicated in liver injury amelioration through enhanced cell proliferation. Kyoto encyclopedia of genes and genomes (KEGG) pathway analysis (Fig. S32†) revealed significant enrichment in pathways associated with liver injury, including the AGE-RAGE signaling pathway in diabetic complications, insulin resistance, and type II diabetes mellitus. Additionally, a comprehensive protein–protein interaction (PPI) analysis was conducted on the 164 identified genes to elucidate key therapeutic targets. A large PPI network comprising 164 nodes and 1029 edges was constructed using the STRING database. Core targets were subsequently identified through network topology analysis in Cytoscape, applying median-based selection thresholds (betweenness centrality > 0.00185581, closeness centrality > 0.412371134, clustering coefficient > 0.489655172). The refined PPI network, consisting of 22 nodes and 52 edges, was then extracted for further analysis (Fig. S33†).

Based on the median threshold (degree > 4), BRAF, PTPN11, JAK2, NFE2L2, MAP2K1, PIK3CG, MAPK14, RAF, and RPS6KB1 were selected as potential drug targets for further molecular docking analysis. Among them, compounds **1**–**3** exhibited the most superior docking energy with BRAF (Fig. S34†). Mechanistically, compounds **2** and **3** docked seamlessly into the structural cleft of BRAF (Fig. 7B and C), with compound **2** forming a covalent bond with Cys531 *via* Michael addition,[33] thereby demonstrating superior pharmacological activity compared to compound **3** and exhibiting a non-dose-dependent effect at low

concentrations. In contrast, compound **1**, which contains two aldehyde and ketone groups, underwent conformational adjustments that altered its binding interactions, stabilizing the protein structure by penetrating the active pocket of BRAF (Fig. 7A). Based on these binding interactions, we hypothesize that vernolignans modulate BRAF activity, thereby facilitating the phosphorylation and activation of downstream MAPK, AGE-RAGE, and ERK1/ERK2 signaling pathways, ultimately promoting hepatocyte proliferation and enhancing glucose metabolism.[34]
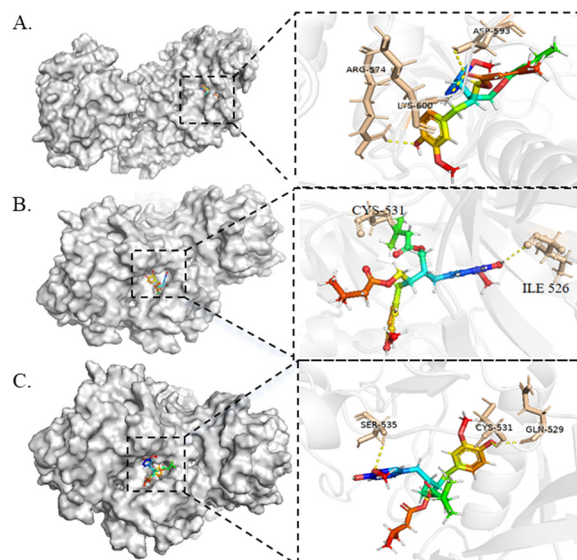

Fig. 7 Molecular docking results of compounds **1**–**3** toward BRAF.

4. Conclusions

In summary, this study successfully isolated three new dibenzylbutane lignans (vernolignans A–C) from *V. cinerea*, along with three known compounds, through a bioactivity-guided isolation process. The structures of the new compounds were elucidated using HR-ESI-MS, 1D and 2D NMR, experimental and calculated ECD, and the AI-based DeepSAT tool, which proved to be highly effective in accelerating structure elucidation. Compounds **2** and **3** demonstrated significant hepatoprotective effects by improving cell viability and reducing APAP-induced ALT levels in murine hepatocytes. Bioinformatics analysis and molecular docking suggested that BRAF might be a potential target for these lignans.

These findings highlight the potential of lignans from *V. cinerea* as therapeutic agents for DILI. Future work should focus on further exploring the *in vivo* efficacy and safety of these compounds, as well as conducting more detailed mechanistic studies to validate the role of BRAF and other potential targets in mediating their hepatoprotective effects. Additionally, the application of AI-driven tools like DeepSAT in natural product research demonstrates significant promise for accelerating the discovery and characterization of bioactive compounds from natural sources.

Data availability

The data supporting this article have been included as part of the ESI,† including NMR spectra of compounds **1**–**6**, alongside MS and CD spectra of compounds **1**–**3**.

Author contributions

M. L., M.-K. Z., and Y.-T. Z. performed the isolation and structural elucidation of natural compounds. X. S. and J. P. contributed to the bioactive evaluation. M.-A. G. contributed to chemical calculation. Y.-S. C. and R.-Y. Y. designed and supervised the project, and edited the manuscript. All authors discussed the results and commented on the manuscript.

Conflicts of interest

There are no conflicts to declare.

Acknowledgements

References

1 M. D. Leise, J. J. Poterucha and J. A. Talwalkar, *Mayo Clin. Proc.*, 2014, **89**, 95–106.

2 N. C. E. S. Raul and J. Andrade, *Nat. Rev. Dis. Primers*, 2019, **5**, 58.

3 M. C. Donnelly, J. S. Davidson, K. Martin, A. Baird, P. C. Hayes and K. J. Simpson, *Aliment. Pharmacol. Ther.*, 2017, **45**, 833–843.

4 A. Reuben, H. Tillman, R. J. Fontana, T. Davern, B. McGuire, R. T. Stravitz, V. Durkalski, A. M. Larson, I. Liou, O. Fix, M. Schilsky, T. McCashland, J. E. Hay, N. Murray, O. S. Shaikh, D. Ganger, A. Zaman, S. B. Han, R. T. Chung, A. Smith, R. Brown, J. Crippin, M. E. Harrison, D. Koch, S. Munoz, K. R. Reddy, L. Rossaro, R. Satyanarayana, T. Hassanein, A. J. Hanje, J. Olson, R. Subramanian, C. Karvellas, B. Hameed, A. H. Sherker, P. Robuck and W. M. Lee, *Ann. Intern. Med.*, 2016, **164**, 724.

5 X. Meng, Y. Li, S. Li, R. Y. Gan and H. B. Li, *Compr. Rev. Food Sci. Food Saf.*, 2018, **17**, 472–495.

6 E. S. Hackett, D. C. Twedt and D. L. Gustafson, *J. Vet. Intern. Med.*, 2013, **27**, 10–16.

7 C. Luangchosiri, A. Thakkinstian, S. Chitphuk, W. Stitchantrakul, S. Petraksa and A. Sobhonslidsuk, *BMC Complementary Altern. Med.*, 2015, **15**, 334.

8 N. J. Toyang and R. Verpoorte, *J. Ethnopharmacol.*, 2013, **146**, 681–723.

9 A. C. Allabi, K. Busia, V. Ekanmian and F. Bakiono, *J. Ethnopharmacol.*, 2011, **133**, 234–243.

10 L. R. Song, *Chinese Herbal Medicine Dictionary*, Jiangsu New Medical College, China, 1977.

11 M. Gupta, U. K. Mazumder, L. Manikandan, P. K. Haldar, S. Bhattacharya and C. C. Kandar, *Fitoterapia*, 2003, **74**, 148–150.

12 G. Miklossy, U. J. Youn, P. B. Yue, M. M. Zhang, C. H. Chen, T. S. Hilliard, D. Paladino, Y. F. Li, J. Choi, J. N. Sarkaria, J. K. Kawakami, S. Wongwiwatthananukit, Y. Chen, D. Q. Sun, L. C. Chang and J. Turkson, *J. Med. Chem.*, 2015, **58**, 7734–7748.

13 C. Monton, P. Kittiratpattana, S. Nakyai, T. Sutapakul, A. Navabhatra, T. Wunnakup, N. Chankana and J. Suksaeree, *Adv. Tradit. Med.*, 2022, **22**, 697–711.

14 G. Leelaprakash, S. Mohan-Dass and V. Sivajothi, *Int. J. Pharm. Sci. Rev. Res.*, 2011, **10**, 30–34.

15 A. Prasopthum, P. Pouyfung, S. Sarapusit, E. Srisook and P. Rongnoparut, *Drug Metab. Pharmacokinet.*, 2015, **30**, 174–181.

16 P. Pouyfung, S. Sarapusit and P. Rongnoparut, *Phytother. Res.*, 2017, **31**, 1916–1925.

17 S. Boonruang, K. Prakobsri, P. Pouyfung, E. Srisook, A. Prasopthum, P. Rongnoparut and S. Sarapusit, *J. Enzyme Inhib. Med. Chem.*, 2017, **32**, 1136–1142.

18 C. Promputta, V. Anupunpisit, G. Anantasomboon, R. Palasoon, A. Wimoonchart and W. Timklay, *J. Curr. Sci. Tech.*, 2024, **14**, 67.

19 M. K. Zhang, X. Yang, Y. Wei, M. Wall, T. Songsak, S. Wongwiwatthananukit and L. C. Chang, *J. Nat. Prod.*, 2019, **82**, 2124–2131.

20 M. K. Zhang, T. P. Kondratyuk, S. G. Cao, M. Li, T. Songsak, S. Wongwiwatthananukit, Y. S. Cai and L. C. Chang, *Org. Lett.*, 2025, **27**, 909–914.

21 W. C. Chen, X. Song, J. Wu, Y. T. Zhong, P. P. Edjah, Q. Y. Zhang, M. Li, K. K. Zhu, C. K. Tian, R. Y. Yuan, X. Y. Wu, P. Gao, K. Hong, M. K. Zhang, J. Ping and Y. S. Cai, *J. Nat. Prod.*, 2025, **88**, 336–348.

22 H. W. Kim, C. Zhang, R. Reher, M. Wang, K. L. Alexander, L. Nothias, Y. K. Han, H. Shin, K. Y. Lee, K. H. Lee, M. J. Kim, P. C. Dorrestein, W. H. Gerwick and G. W. Cottrell, *Aust. J. Chem.*, 2023, **15**, 71.

23 S. Jasial, Y. Hu, M. Vogt and J. Bajorath, *F1000Research*, 2016, **5**, 591.

24 Y. Luo, X. X. Zheng, M. J. Qiu, Y. P. Gou, Z. X. Yang, X. B. Qu, Z. Chen and Y. Q. Lin, *Prog. Nucl. Magn. Reson. Spectrosc.*, 2025, **146**, 101556.

25 Z. K. Duan, X. Wang, M. Y. Lian, S. S. Guo, Z. H. Gao, M. Bai, X. X. Huang and S. J. Song, *J. Agric. Food Chem.*, 2024, **72**, 10958–10969.

26 B. Ryu, E. Glukhov, T. R. Teixeira, C. R. Caffrey, S. Madiyan, V. Joseph, N. E. Avalon, C. A. Leber, C. B. Naman and W. H. Gerwick, *J. Nat. Prod.*, 2024, **87**, 1601–1610.

27 K. L. Alexander, C. B. Naman, A. Iwasaki, A. Mangoni, T. Leao, R. Reher, D. Petras, H. Kim, E. Ternon, E. J. E. Caro-Diaz, E. Glukhov, J. A. Mitrevska, N. E. Avalon, B. M. Duggan, L. Gerwick and W. H. Gerwick, *J. Nat. Prod.*, 2025, **88**, 322–335.

28 F. Bohlmann, M. Lonitz and K. H. Knoll, *Phytochemistry*, 1978, **17**, 330–331.

29 Y. Nakasone, K. Takara, K. Wada, J. Tanaka, S. Yogi and N. Nakatani, *Biosci., Biotechnol., Biochem.*, 1996, **60**, 1714–1716.

30 H. C. Jeh-Jian Hsiao, *Phytochemistry*, 1995, **39**, 899–902.

31 Z. D. Wu, Y. J. Lai, L. Zhou, Y. Wu, H. C. Zhu, Z. X. Hu, J. Yang, J. W. Zhang, J. P. Wang, Z. W. Luo, Y. B. Xue and Y. H. Zhang, *Sci. Rep.*, 2016, **6**, 24809.

32 F. Bohlmann, C. Zdero, R. M. King and H. Robinson, *Phytochemistry*, 1982, **21**, 1045–1048.

33 Y. Liu, Q. Guo, H. Yang, X. W. Zhang, N. Feng, J. K. Wang, T. T. Liu, K. W. Zeng and P. F. Tu, *ACS Cent. Sci.*, 2022, **8**, 1102–1115.

34 R. Roskoski, *Pharmacol. Res.*, 2012, **66**, 105–143.